J Solid State Electrochem (2012) 16:1141–1149
DOI 10.1007/s10008-011-1497-2

ORIGINAL PAPER

Energy level alignment at interfaces between 3-(4-biphenylyl)-4-phenyl-5-(4-tert-butyl phenyl)-1, 2, 4-triazole (TAZ) and metals (Ca, Mg, Ag, and Au): experiment and theory

Mahesh Datt Bhatt · Akihisa Baba · Takeaki Sakurai · Katsuhiro Akimoto

Received: 7 April 2011 / Revised: 7 June 2011 / Accepted: 29 June 2011 / Published online: 22 July 2011

Abstract We have performed ultraviolet photoelectron spectroscopy measurements and density functional theory calculations to study the electronic structure at the interface between organic semiconductor (3-(4-biphenylyl)-4-phenyl-5-(4-tert-butyl phenyl)-1,2,4-triazole (TAZ)) and metals (Ca, Mg, Ag, and Au). The basic mechanism of interface states at organic–metal interfaces can be understood by controlling the injection of charge carriers at these interfaces. The position of highest occupied molecular orbital relative to the Fermi level and the magnitude of the interface dipole are measured for each organic–metal interface. For TAZ on Ca, Mg, and Ag, interface states are observed near the Fermi level. However, no interface state is observed for TAZ on Au. It is analyzed qualitatively that the interface state is formed due to interaction of TAZ lowest unoccupied molecular orbital composed of C2p and metal s levels. It is suggested that the interface state plays an important role in charge transport at the interface. The mechanism of formation of interface states and electrical properties are discussed.

Keywords TAZ · Electronic structure · Energy · Organic device · Buffer layer · Work function

A. Baba · T. Sakurai · K. Akimoto
Institute of Applied Physics, University of Tsukuba, Tsukuba, Ibaraki 305-8577, Japan

M. D. Bhatt (✉)
WCU Multiscale Engineering Division, School of Mechanical and Aerospace Engineering, Seoul National University, Seoul 151-742, South Korea
e-mail: mbhatt54@yahoo.com

Introduction

Organic semiconductors based on π-conjugated molecules are promising candidates for a number of opto-electronic devices, such as organic light-emitting diodes (OLEDs) or organic field-effect transistors (OFETs) [1–3]. These organic semiconductors have been widely studied both experimentally [4, 5] and theoretically [6–9], giving considerable insight into the intrinsic electronic and optical properties of the active organic layers. The operation of an organic device (OLED or OFET or OPV) is crucially determined by the interface between a metal electrode and organic semiconductor. The electrical properties at organic–metal interfaces influence greatly the device performance. One of the methods to improve the interface properties by introduction of buffer layer, for example, 2,9-dimethyl-4,7-diphenyl-1,10-phenanthroline (BCP) between an organic semiconductor and a metal electrode in electronic devices [10–14]. Besides such buffer layers, there is an important electron transport and hole blocking another material namely 3-(4-biphenylyl)-4-phenyl-5-(4-tert-butyl phenyl)-1,2,4-triazole (TAZ), which plays an important role as active function in some highly efficient devices [15–19]. The chemical structure of TAZ is shown as in Fig. 1. TAZ is an electron transport and hole-blocking material having energy difference of 3.3 eV between highest occupied molecular orbital (HOMO) and lowest unoccupied molecular orbital (LUMO). The HOMO level of TAZ is situated at 6.6 eV deep below the vacuum level; therefore, TAZ can be used as a hole-blocking layer. TAZ plays an important role in light-emitting devices by increasing the possibility of charge recombination; however, the charge separation/recombination mechanism is not clear

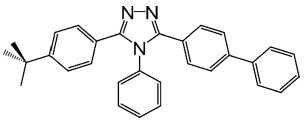

Fig. 1 Chemical structure of TAZ

yet. In this paper, the electronic structure of the interface between TAZ and a metal has studied by both experimental (ultraviolet photoelectron spectroscopy, UPS) and theoretical (density functional theory, DFT) methods.

Experimental details

All depositions and measurements are performed in an ultrahigh vacuum system composed of a UPS measurement chamber with a base pressure of 1.6×10^{-8} Pa and a preparation chamber for TAZ and metal deposition with a base pressure of 1.0×10^{-7} Pa. The substrates used for all three samples are Au films deposited on Si (100) wafers. Four metals Ca, Mg, Ag, and Au are used as electrode materials and deposited on the substrates at room temperature. The organic compound (TAZ) is purified by vacuum sublimation at room temperature at the rate of 0.1 Å/s. The pressure during the sublimation is kept less than 1.0×10^{-5} Pa. The thickness of TAZ is varied from 4 to 100 Å.

The UPS measurements are performed at the beam line 11D in KEK photon factory. The photon energy is maintained at 65.12 eV. The resolution is determined from the width of the Fermi level in the UPS spectrum of Au and was found to be 400 meV. The samples are biased at −4 V to obtain the vacuum level from the secondary electron cutoff of the spectrum. The photon incidence angle is fixed at 45° and the detection angle is adjusted normal to the sample surface.

Computational methodology

Ca (111), Mg (111), Ag (111), and Au (111) surfaces are constructed using 13 metal atoms having the same arrangement for all metals in *x*–*y* axes plane as shown in Fig. 2a. The atomic distances are kept constant with 0.394, 0.319, 0.289, and 0.288 nm for Ca, Mg, Ag, and Au, respectively, which are the same as those of the bulk values. The small metal clusters are chosen in our calculations due to the fact that their work functions are found to be close to their experimental values and our purpose of this research is to investigate the chemical trend in the interaction of TAZ with various kinds of metals qualitatively. A single TAZ molecule is basically kept in parallel with a metal (111) surface in a flat-lying manner because there are several works reporting energetically stable configuration as flat-lying geometry in polycyclic molecules on metal surface [20]. The atomic arrangement for the case of TAZ on Ca in *x*–*y* axes plane is shown in Fig. 2b.

In the first step of our calculations, we have fixed the metal atoms and moved rigidly the TAZ molecule in *x*–*y* axes plane, keeping it at a constant distance from the metal surface and also twisted around at the same time to find the adsorption configuration which minimizes the total energy for the system and provide a starting point for a more accurate analysis [20] with PCGAMESS/Firefly software package [21]. In the next step, we have performed our calculations with varying interplanar distance between TAZ and metal surface, that is, *z*-axis, within the density functional theory, where the exchange correlation function has been parameterized according to the generalized gradient approximation in the Becke [22] and Lee–Yang–Parr [23] (B3LYP5). The hybrid parameter consists of B3LYP as implemented in GAMESS (US), using VWN formula 5 [24] correlations. The basis set 6–31+G** was chosen for C, N, and H atoms of isolated BCP molecule as well as for metals Ca, Mg, and core frozen basis set SBKJC+** for Ag, Au junctions with one TAZ molecule to give the result in consistent with UPS results. These calculations are performed in restricted Hartree–Fock mode for closed-shell metal such as Ca and Mg; while in restricted open Hartree–Fock mode for open shell metals such as Ag and Au. The approximate basis set superposition error [25] for all TAZ/metal systems using both basis sets 6–31+G** and SBKJC+**, is calculated by counter poise method and is observed to be negligibly small.

Results and discussions

Experimental (UPS) results

The UPS spectra of TAZ on (a) Ca, (b) Mg, (c) Ag, and (d) Au obtained on the basis of the Fermi level position are shown in Fig. 3. It is analyzed that UPS spectra are almost the same for all cases of TAZ of thickness 100 Å, assuming the spectra of bulk TAZ. No interface state is formed near the Fermi level for TAZ on Au due to very weak interaction between TAZ and Au; however, two new peaks known as "interface states" are observed for TAZ on Ca, Mg, and Ag. The cutoff position of each spectrum shifts with increasing TAZ thickness. The shift values are indicated by Δ in Fig. 3. The cutoff position shift means the vacuum level shift of TAZ on metals. The vacuum level shifts are 0.5, 1.2, 1.8, and 1.9 eV for Ca, Mg, Ag, and Au respectively. The energy level diagrams for TAZ on (a) Au, (b) Ag, (c) Mg, and (d) Ca are shown as in Fig. 4. We analyze that the pseudowork function of TAZ is almost constant and shift of the HOMO level towards a high binding energy with decrease in metal work function. The positions of LUMO

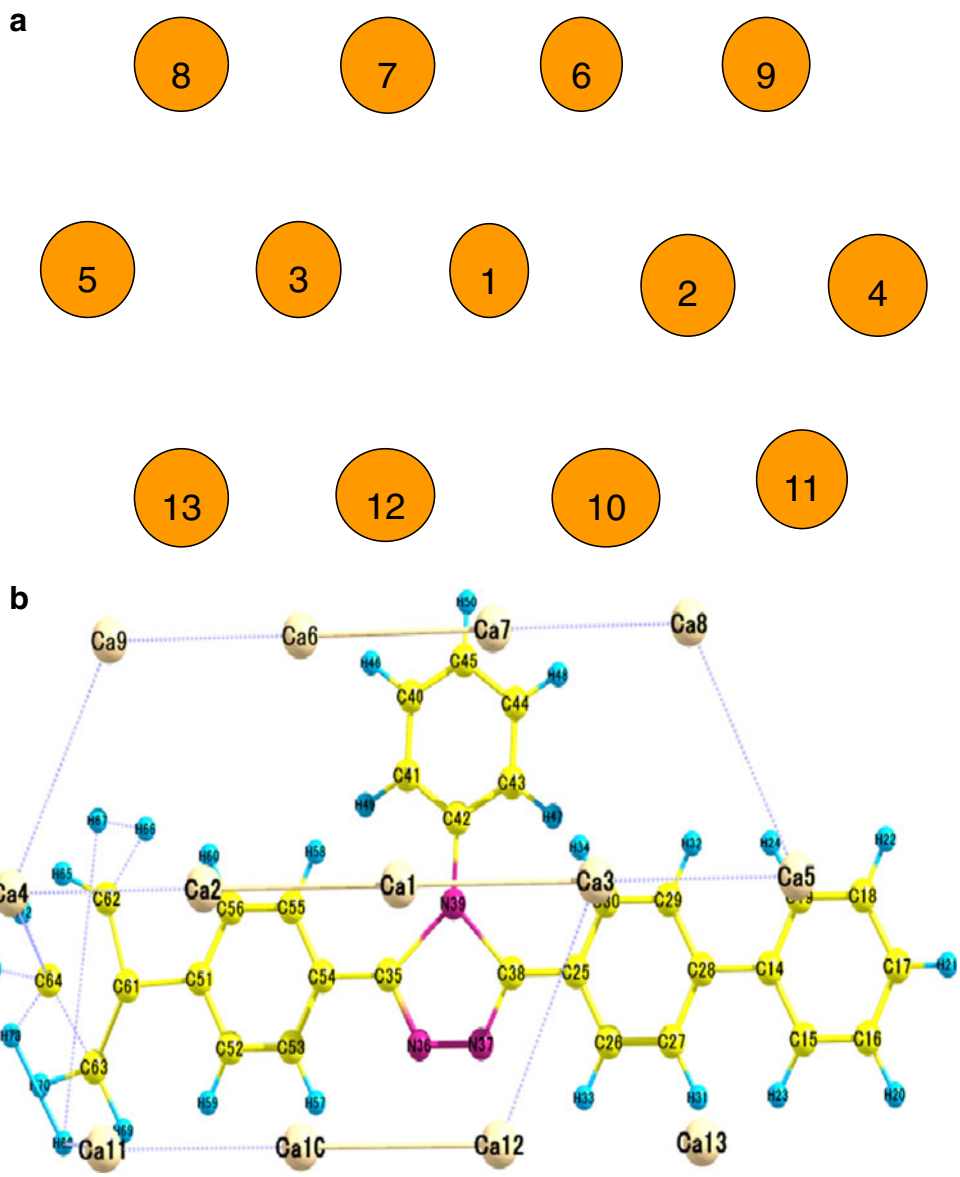

Fig. 2 Atomic geometry of metal (111) surface (**a**), and top view of TAZ molecule on metal substrate in case of TAZ on Ca (**b**)

of TAZ on Ca, Mg, Ag, and Au can be determined according to the metal Fermi level. In case of TAZ on metals, TAZ LUMO seems to be important for charge injection at the interface because it plays an important role to generate interface state for TAZ on metals other than Au. These findings suggest the importance of chemical interaction of TAZ with these metals.

Calculation (DFT) results

The structure of TAZ on metal is obtained by evaluating bond energy, E_b (TAZ/metal), using the equation: E_b (TAZ/metal)$=E_{total}$(TAZ+metal)$-E_{total}$(TAZ)$-E_{total}$(metal), where E_{total}(TAZ+metal), E_{total}(TAZ), and E_{total}(metal) denote the total energies of the adsorbed system, of the isolated TAZ molecule, and of the metal substrate, respectively [20]. The binding energy versus interplanar distance, d, was plotted around the equilibrium distances for TAZ on Ca and Au, and the equilibrium distances were found to be 0.28 and 0.30 nm for Ca and Au as shown in Figs. 5a, b, respectively. In the same way, the equilibrium distance for Mg and Ag was obtained to be 0.27 and 0.28 nm. The binding energies for all TAZ/metal systems, corrected by basis set superposition error [20] using counter poise method, found to be almost similar to the binding energy calculated initially with basis sets 6–31+G** for metals Ca, Mg, and SBKJC+** for metals Ag, Au. The experimental metal–metal distances, calculated equilibrium distances between TAZ and metal (111) surfaces, optimized binding energies, magnitude of charge transfer calculated according to Bader analysis, and calculated and experimental metal work functions, are given in Table 1. The

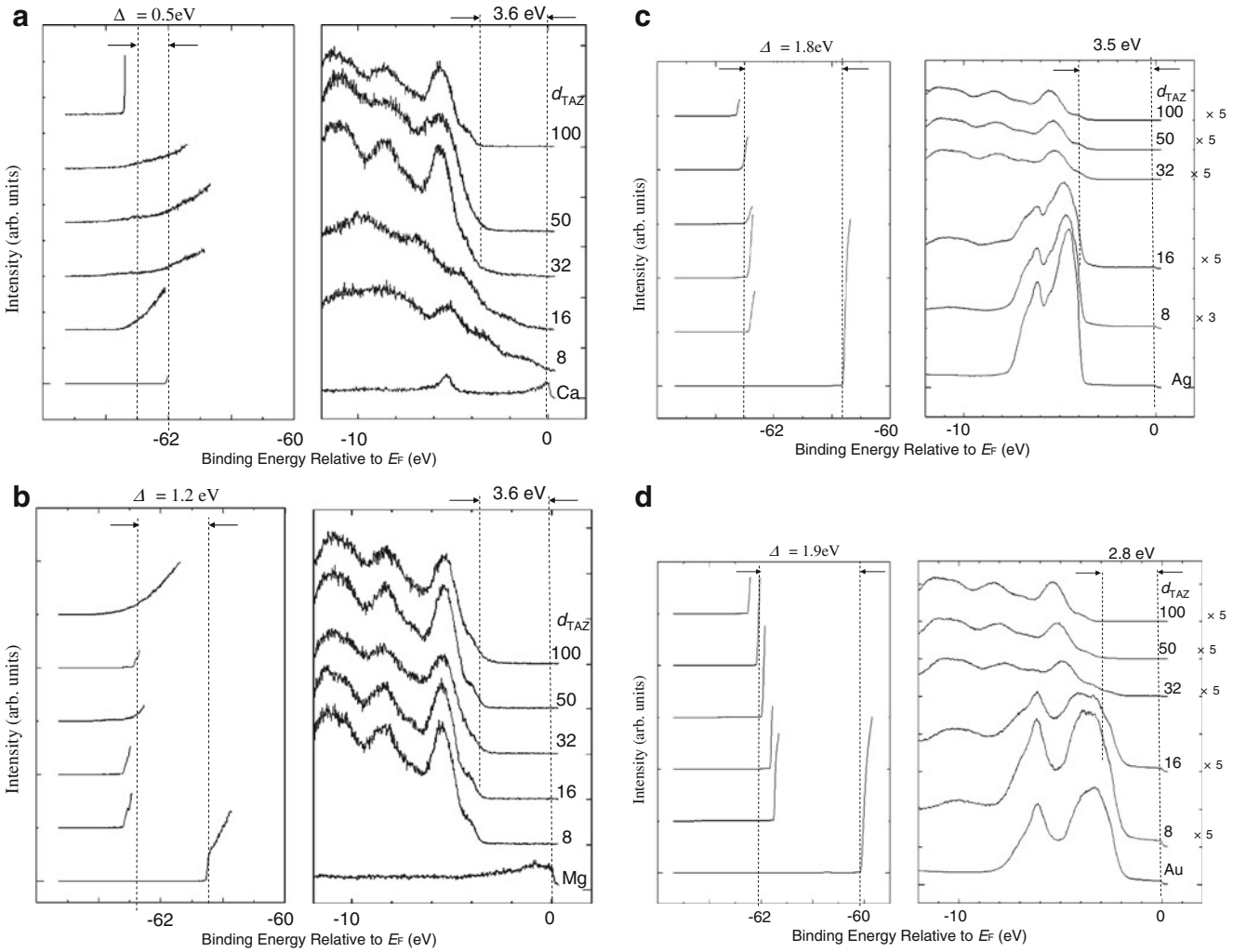

Fig. 3 UPS spectra of TAZ on Ca (**a**), TAZ on Mg (**b**), TAZ on Ag (**c**), and TAZ on Au (**d**)

calculated work functions of metals are found to be nearly consistent with their experimental values except for Au. Therefore, the cluster model used in this study may be effective to discuss the chemical trend of the electronic structure qualitatively. The calculated binding energy, E_b, at the equilibrium distance for TAZ on Ca is about −4.25 eV; the negative value suggests that the process is exothermic and therefore energetically more stable than the two separate constituents. The E_b value decreased with decreasing work function of metals and the binding energy for TAZ on Au is about +2.27 eV. Such small positive binding energy for TAZ on Au indicates the less stable system.

The binding energy and the square of transferred charge versus work functions of metals for TAZ/metal

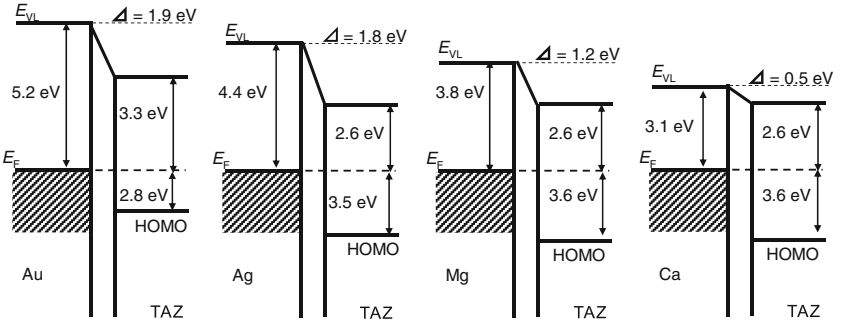

Fig. 4 Energy diagrams for TAZ on (**a**) Au, (**b**) Ag, (**c**) Mg, and (**d**) Ca based on UPS measurements

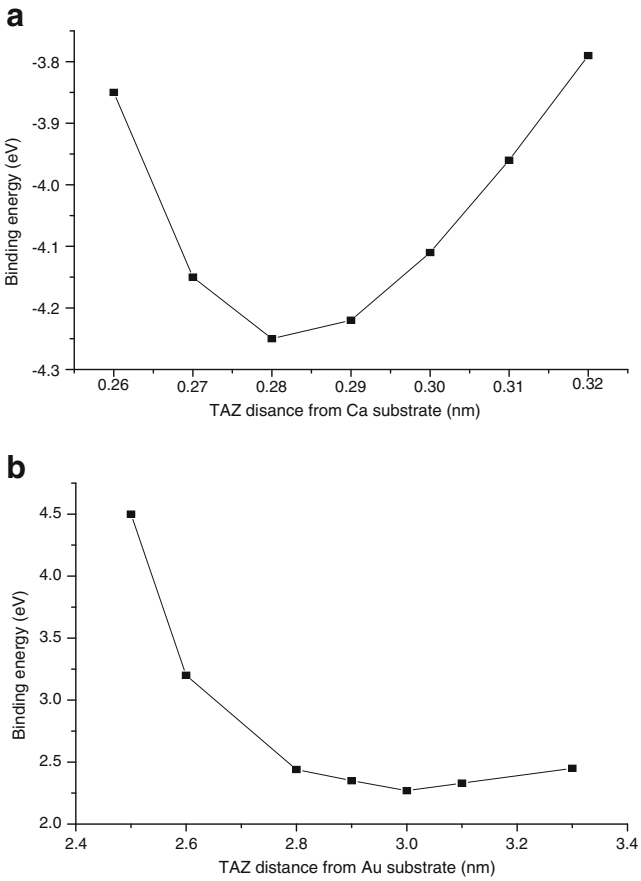

Fig. 5 Binding energy vs. planar distance of CBP on Ca (**a**) and Au substrate (**b**)

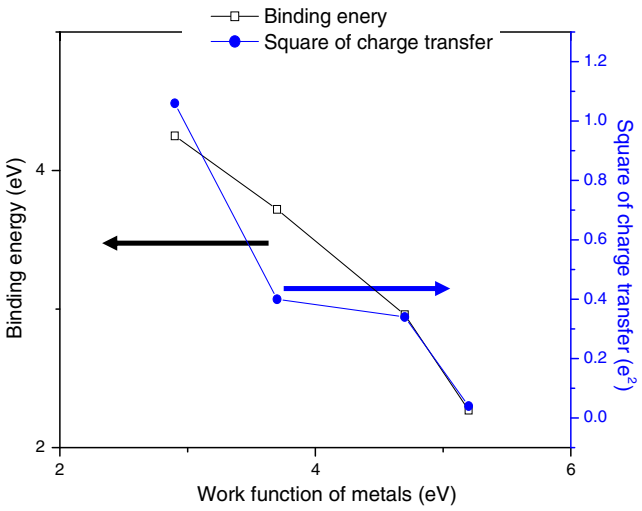

Fig. 6 Binding energy and square of charge transfer versus work function of metals

systems are shown in Fig. 6. The binding energy decreases gradually with decreasing metal work function. The square of transferred charge also decreases gradually with decreasing metal work function similar to the binding energy. Since the square of charge is proportional to the Coulomb interaction and since the equilibrium distances between TAZ and metal surfaces are roughly the same, therefore, contribution of ionic interaction in the binding energy between TAZ and metals seems to be relatively large.

Figure 7a–e show the DFT density of states of Ca (111) surface (a), Mg (111) surface (b), Ag (111) surface (c), Au (111) surface (d), and isolated TAZ molecule (e) obtained according to the molecular levels broadened by Gaussian broadening with the full width at half maximum of 0.5 eV for each molecular level. The density of states of Ca, Mg, Ag, and Au obtained by DFT are almost the same as those obtained by UPS in the energy range below the Fermi level. The experimental HOMO–LUMO gap of TAZ is reported to be about 3.3 eV and the calculated value in this work is 3.3 eV as shown in Fig. 7e. As mentioned above, calculated metal work functions in this work are roughly consistent with the experimental values, and the calculated HOMO–LUMO gap is also consistent with the experimental one, therefore, the simulation models used in this study can be considered to be good enough to investigate the interaction of TAZ with metals qualitatively.

Figure 7f–i show the simulation results of TAZ on metal systems for TAZ on Ca (111) surface (f), TAZ on Mg (111) surface (g), TAZ on Ag (111) surface (h), and TAZ on Au (111) surface (i). It should be noted that two interface states are appeared between E_F and HOMO for TAZ on Ca, Mg, and Ag; however, no interface state was observed for TAZ on Au. To confirm the appearance of such interface states,

Table 1 Metal atomic distances, TAZ–metal equilibrium distances, optimized binding energies, magnitude of charge transfer according to Bader analysis, calculated and experimental values of metal work functions are listed

Substrate metals	Metal atomic distance (nm)	TAZ–metal equilibrium distance (nm)	Binding energy (eV)	Charge transfer (|e|)	Work function	
					Calculated (eV)	Experimental (eV)
Ca	0.394	0.28	−4.25	1.07	2.50	2.90
Mg	0.319	0.27	−3.72	0.66	3.08	3.70
Ag	0.289	0.30	+2.96	0.59	4.04	4.73
Au	0.288	0.28	+2.27	0.19	5.33	5.20

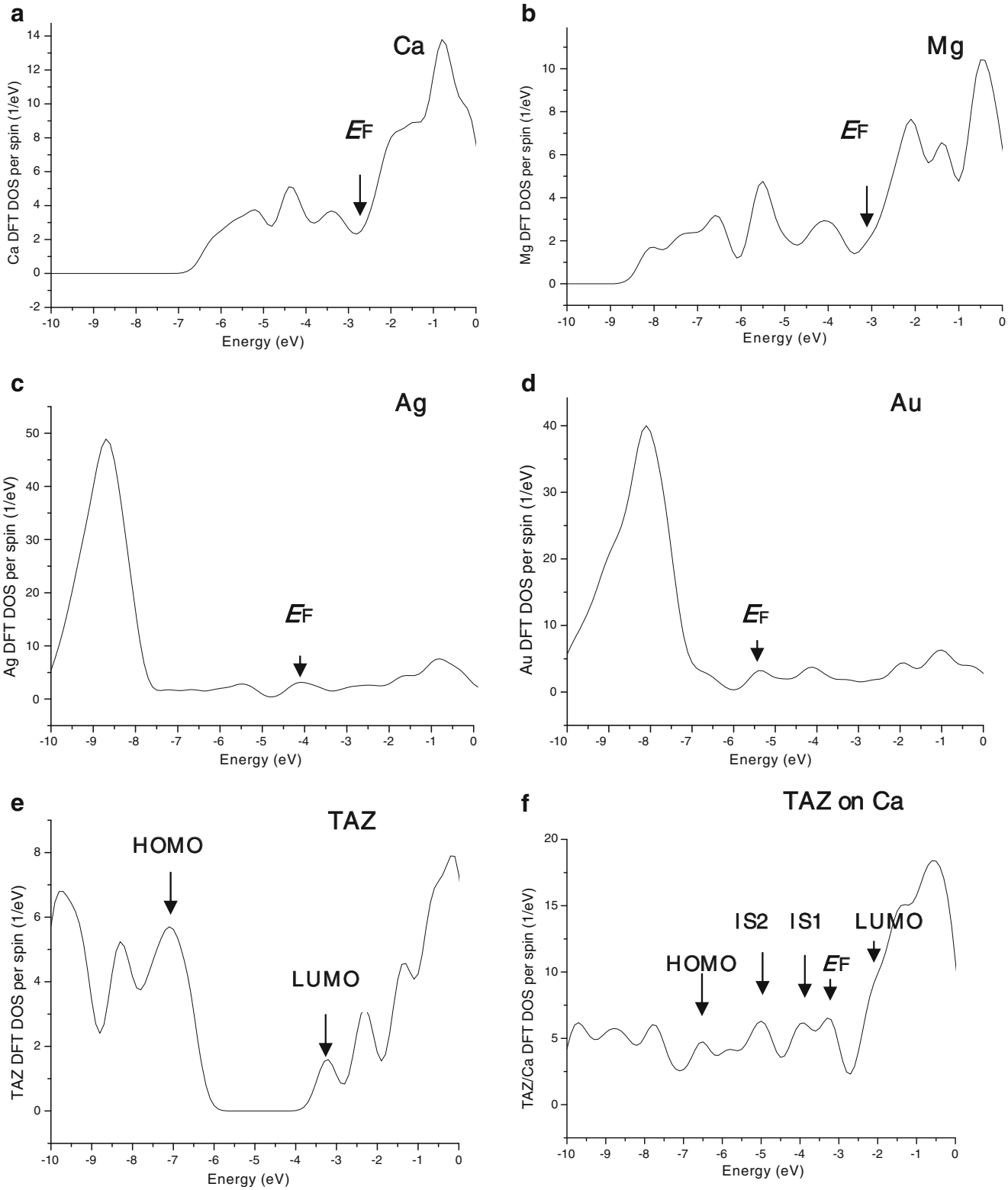

Fig. 7 Density of states obtained by DFT for Ca (**a**), Mg (**b**), Ag (**c**), Au (**d**), TAZ (**e**), TAZ on Ca (**f**), TAZ on Mg (**g**), TAZ on Ag (**h**), and TAZ on Au (**i**)

difference spectra between TAZ on metal system and metal surfaces are shown in Fig. 8a–d. The two interface states are clearly observed near the Fermi level for TAZ on Ca, Mg, and Ag systems; however, no interface state is observed for TAZ on Au system. These results are fairly consistent with the UPS results.

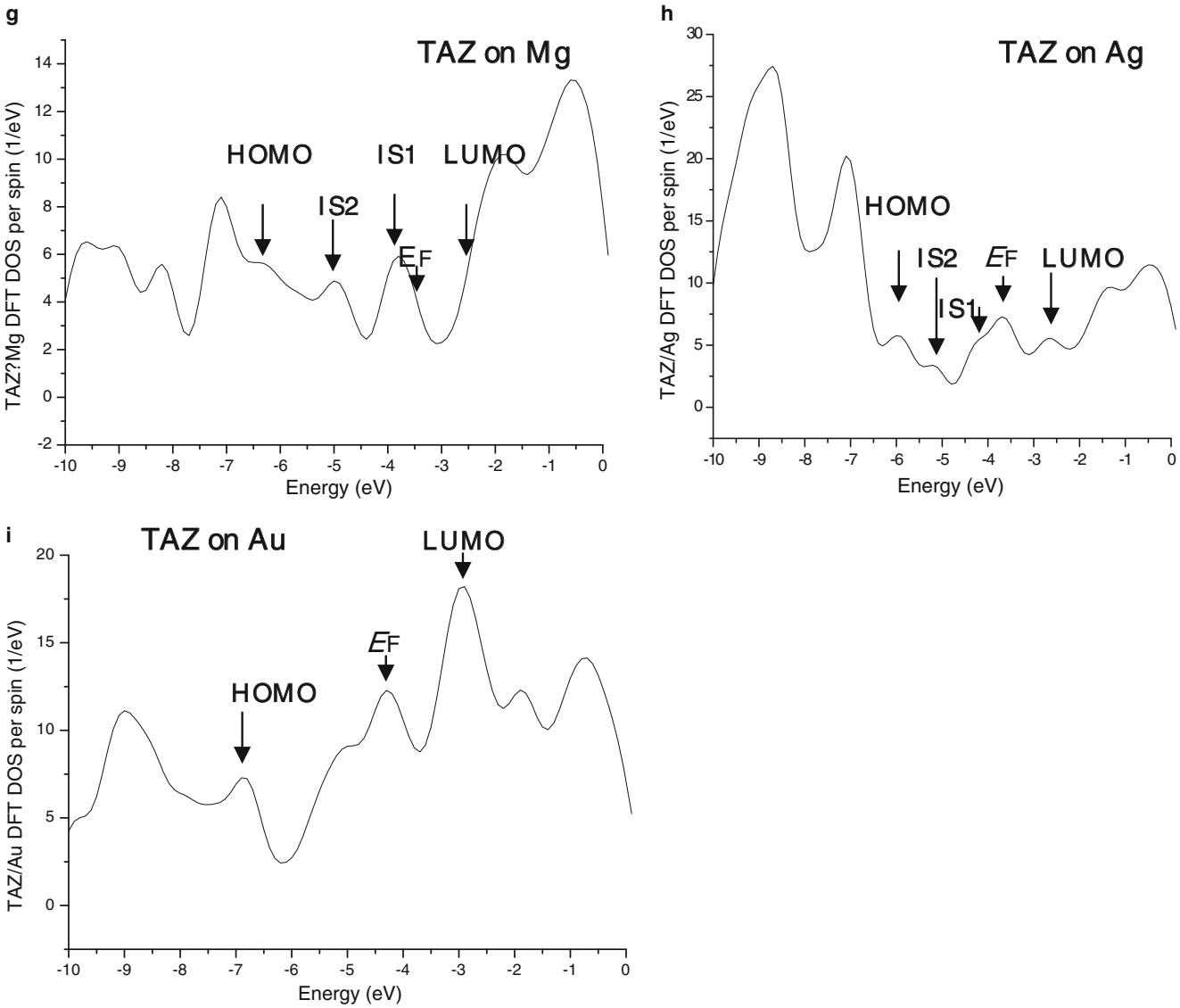

Fig. 7 (continued)

The major atomic components for TAZ on metal system for the molecular orbitals of HOMO, LUMO, and the Fermi level were examined by analyzing atomic orbital coefficient and atomic component ratio A_i:Z_i derived from TAZ and metal, respectively, was extracted, where A_i was defined as,

$$A_i = \sum_{\mu} C_{\mu i}^{\ 2},$$

and $C_{\mu i}$ is the coefficients of the μth basis function in the *i*th molecular orbital, and the μth basis function is considered only for carbon 2*s* and 2*p* orbitals of TAZ. Similarly, Z_i was defined as,

$$Z_i = \sum_{\mu} C_{\mu i}^{\ 2},$$

and the μth basis function is considered only for *s* and *p* orbitals of metal. The atomic orbital component ratios derived from TAZ and metal, A_i:Z_i, for the molecular orbitals of HOMO, Fermi level, and LUMO are listed in Table 2.

As shown in Table 2, for the TAZ on Au system, the HOMO and LUMO are composed mainly of TAZ derived atomic orbitals, however, a small contribution from TAZ to the Fermi level is observed. Such less orbital mixing is consistent with the estimation of small binding energy as shown in Table 1. For TAZ on Ca, Mg, and Ag systems, the orbital mixing becomes significant, especially in the Fermi level and LUMO. Such orbital mixing increases with decrease in the metal work function. The contribution of carbon atomic orbitals and metal atomic orbitals for LUMO is almost even. When we consider the electron transport

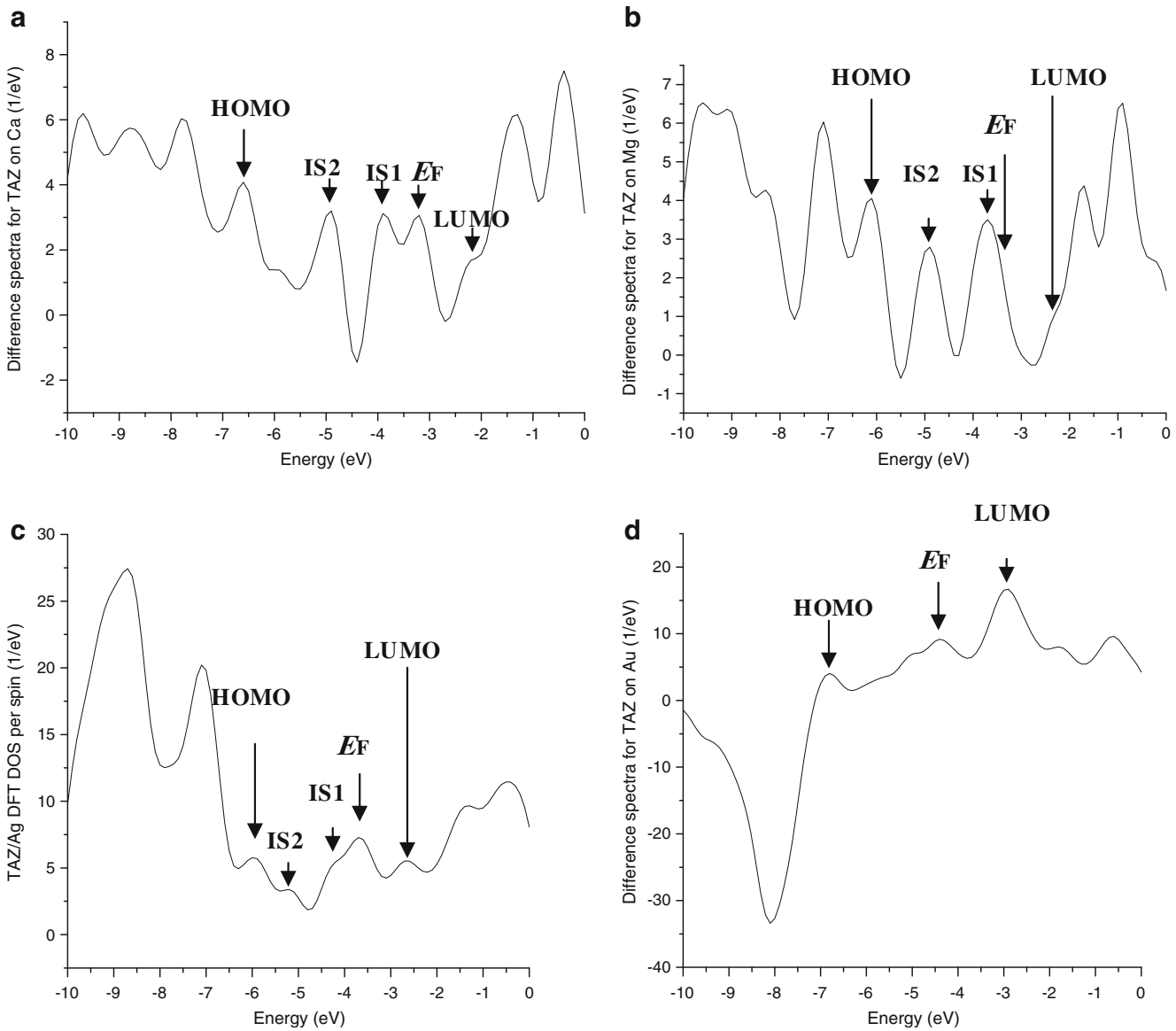

Fig. 8 Difference spectra for **a** TAZ on Ca, **b** TAZ on Mg, **c** TAZ on Ag, and **d** TAZ on Au

Table 2 Atomic component ratio A_i: Z_i, where A_i and Z_i are defined as $A_i = \sum_{\mu} C_{\mu i}^2$, and $C_{\mu i}$ is the coefficients of the μth basis function in the *i*th molecular orbital, and the μth basis function is considered only for carbon 2*s* and 2*p* orbitals in TAZ

TAZ/metal	HOMO	Interface states		E_F	LUMO
		IS1	IS2		
TAZ/Ca	0.96:0.04	0.34:0.66	0.31:0.69	0.48:0.52	0.49:0.51
TAZ/Mg	0.94:0.06	0.35:0.65	0.30:0.70	0.49:0.51	0.47:0.53
TAZ/Ag	0.97:0.03	0.32:0.68	0.29:0.71	0.47:0.53	0.46:0.54
TAZ/Au	0.97:0.03			0.05:0.95	0.91:0.09

$Z_i = \sum_{\mu} C_{\mu i}^2$, and the μth basis function is considered only for *s* and *p* orbitals in metal

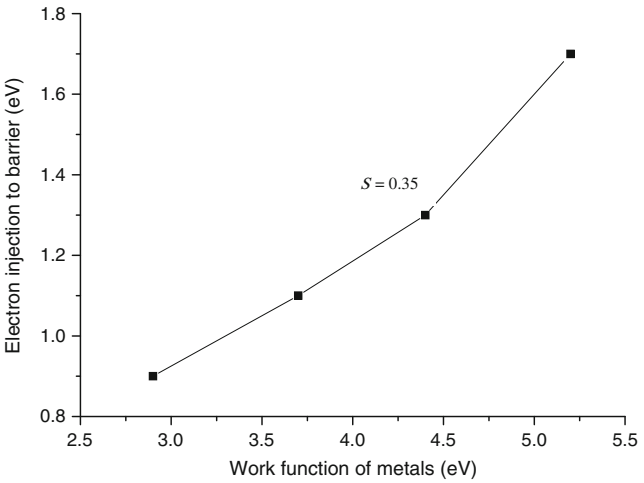

Fig. 9 Plot of barrier height of electrons versus work function of metals

between TAZ and metal electrodes, we should remark the continuity of the wave function at the interface. For TAZ on Ca, Mg, Ag systems, the LUMO and Fermi level are composed of both TAZ and metal-derived orbitals; therefore, the wave function at the interface is connected continuously between TAZ and metal. On the other hand, for TAZ on Au, the wave function at the interface is hardly connected continuously. Such continuity of the wave function at the interface between TAZ and metal is in good agreement with the results of electron transport properties obtained experimentally.

Figure 9 shows the relationship between the experimental metal work function and the energy difference of [LUMO–Fermi level] which corresponds to a barrier height for electrons. The barrier heights for TAZ on metals vary strongly with metal work functions. The reason for such strong variation of barrier heights with work functions of metals is not clear at present; however, interaction between LUMO of TAZ and the Fermi level of metal may play an important role in determining the barrier height.

Conclusions

The electronic structure at the interfaces between TAZ and metals (Ca, Mg, Ag, and Au) are studied by both UPS measurements and DFT calculations. Each interface is studied by depositing TAZ on metals. We find the increasing values of interface dipole for all four interfaces, which clearly indicates that the position of the Fermi level varies strongly with the metal work function, in the TAZ molecular gap.

The electronic structures of the interface between TAZ and metal surfaces; Ca (111), Mg (111), Ag (111), and Au (111) which is composed of 13 atoms, are investigated by DFT. In the case of TAZ on Au, the bond energy and charge transfer were found to be small, however, for TAZ on Ca, Mg, and Ag, the bond energy and charge transfer increase with decreasing metal work function. For TAZ on Ca, Mg, and Ag systems, orbital mixing occurs. On the other hand, for TAZ on Au system, orbital mixing does not occur. Such orbital mixing may play an important role in electron transport at the interface between TAZ and metal.

References

1. D Fichou, C Ziegle (1999) Handbook of oligo- and polythiophenes. Ed. D. Fichou, Wiley-VCH, Weinheim, pp 183–282
2. Sirringhaus H, Tessler N, Friend RH (1998) Science 280:1741
3. Gigli G, Inganas O, Anni M, De Vittorio M, Cingolani R, Baibarella G, Favarctto L (2001) Appl Phys Lett 78:1493
4. Horowitz G, Kouki F, Valat P (1999) Phys Rev B 59:10651
5. Pope M, Swenberg CE (1999) Electronic processes in organic crystals and polymers. Oxford University Press, New York
6. Bussi G, Runi A, Molinari E, Caldas MJ, Puschnig P, Ambrosch-Draxl C (2002) App Phys Lett 80:4118
7. Cheng YC, Silbey RJ, da Silva Filho DA, Calbert JP, Cornil J, Bredas JL (2003) J Chem Phys 118:3764
8. Tiago ML, Northrup JE, Louie SG (2003) Phys Rev B 67:115212
9. Hummer K, Ambrosch-Draxl C (2005) Phys Rev B 72:205205
10. Ishii H, Sugiyama K, Ito E, Seki K (1999) Adv Mater (Weinheim, Germany) 11:605
11. Ishii H, Oji H, Ito E, Hayashi N, Yoshimura D, Seki K (2000) J Lumin 87–89:61
12. Ishii H, Hayashi N, Ito E, Washizu Y, Sugi K, Kimura Y, Niwano M, Ouchi Y, Seki K (2004) Phys Status Solidi A 201:1075
13. Song QL, Li FY, Yang H, Wu HR, Wang XZ, Zhou W, Zhao JM, Ding XM, Huang CH, Hou XY (2005) Chem Phys Lett 416:42
14. Yang Y, Teng F, Zhou Q, Wang Y (2006) Appl Surf Sci 252:2355
15. Kido J, Ohtaki C, Hongawa K, Okuyama K, Nagai K (1993) Jpn J Appl Phys 32:917
16. Kido J, Hongawa K, Okuyama K, Nagai K (1993) Appl Phys Lett 63:2627
17. Kido J, Hongawa K, Okuyama K, Nagai K (1994) Appl Phys Lett 64:815
18. Burrows PE, Forrest SR, Thompson ME (1997) Curr Opin Solid State 2:236
19. Lee CL, Lee KB, Kim JJ (2000) Appl Phys Lett 77:2280
20. Picozzi S, Pecchia A, Gheorghe M, Carlo A, Lugli P, Delley B, Elstner M (2003) Phys Rev B 68:195309
21. Schmidt MW, Baldridge KK, Boatz JA, Elbert ST, Gordon MS, Jensen JH, Koseki S, Matsunaga N, Nguyen KA, Su S, Windus TL, Dupuis M, Montgomery JA (1993) J Comput Chem 14:1347
22. Pogrebnaya TP, Becke AD (1988) Phys Rev A 38:3098
23. Lee C, Yang W, Parr RG (1988) Phys Rev B 37:785
24. Vosko SH, Wilk L, Nusair M (1980) Canad J Phys 58:1200
25. Boys SF, Bernardi F (1970) Mol Phys 19:553